Molecular alignment in molecular fluids induced by coupling between density and thermal gradients

Christopher D. Daub,[1,*] Joakim Tafjord,[1]
Signe Kjelstrup,[1] Dick Bedeaux,[1] and Fernando Bresme[2,1]

[1]*Department of Chemistry, Norwegian University of Science and Technology (NTNU), Trondheim, Norway NO-7491*

[2]*Department of Chemistry, Imperial College London, SW7 2AZ, London, UK*

(Dated: February 22, 2016)

Abstract

We investigate, using non-equilibrium molecular dynamics simulations and theory, the response of molecular fluids confined in slit pores under the influence of a thermal gradient and/or gravity-like fields. The gravity-like field induces an inhomogeneous density in the confined fluid, which results in a net orientation of the molecules with respect to the direction of the field. The orientation is qualitatively similar to that induced by a thermal gradient. We find that the average degree of orientation is proportional to the density gradient of the fluid in the confined region and that the orientation increases with the magnitude of the force. The concurrent application of the external gravity-like field and the thermal gradient allows us to disentangle the different mechanisms leading to the thermal orientation of molecular fluids. One mechanism is connected to the density variation of the fluid, while the second mechanism can be readily observed in molecular fluids consisting of molecules with mass or size asymmetry, even in the absence of a density gradient, hence it is connected to the application of the thermal gradient only.

PACS numbers:

*Electronic address: christopher.daub@ntnu.no

I. INTRODUCTION

Molecular fluids are widely used in industrial processes as solvents, and in applications concerned with heat management, and they can be exposed to large thermal gradients. In ionic solutions, the thermal gradient affects the transport of the solute ions (Soret effect) [1]. However, notwithstanding the large amount of work that has been done on the response of polar fluids to external electric fields [2] the intrinsic response of the pure solvent to an applied external field such as a thermal gradient is largely unknown. A better understanding of the non-equilibrium response of these solvents under thermal and/or chemical potential gradients is important to advance their use in applications concerned with fluid transport [3] or heat dissipation and conduction [4] at both nano- and macro-scales.

Recently we discovered that thermal gradients can couple with the internal degrees of freedom of molecules featuring asymmetry in size and/or mass. The coupling results in a preferred orientation of the fluids, where one of the atomic sites in diatomic molecules points towards a hot or a cold source [5]. This phenomenon, which was called "thermo-molecular orientation" (TMO), can be understood in terms of non-equilibrium thermodynamics (NET). Further it was shown in Ref. 5 that the orientation of the molecules follows closely the mass and size dependence of the Soret coefficient in binary mixtures [6, 7]. Simulations indicate that in simple fluids heavy particles tend to accumulate in the cold region. Similarly, in heterogeneous molecules, the heavier site points preferentially towards the cold region. This correlation between the TMO and Soret effects provides a strong guiding principle for the rationalisation and prediction of the preferred orientation of molecules under thermal gradients. Diatomic molecules with slightly different geometries and atomic partial charges that lead to net molecular dipoles have also been studied [8]. In this case the orientation results in a concomitant polarization of the fluid. This polarization is similar to that found in water, an effect that was first reported in Ref. 9 and studied further in subsequent works [10–14].

The theoretical interpretation of molecular orientation under thermal gradients relies on the phenomenological interpretation of non-equilibrium thermodynamics [15]. NET provides a route towards establishing whether coupling effects are possible. However this theory does not provide a microscopic mechanism to explain the origin of such coupling. Computer simulations provide a route to tackle this problem. Indeed, the recently discovered link

between the TMO and the Soret effect [5] is a first step towards advancing our molecular understanding of thermal orientation effects. Further, simulations have been used recently to advance our understanding of the microscopic mechanism leading to the thermal polarization of water [14].

The TMO effects investigated so far were observed in systems that involve both thermal and density gradients. This raises some interesting questions, which we would like to address in this work. How does the density gradient itself contribute to the TMO response, and can we observe molecular orientation in a fluid in the absence of a density gradient? These are fundamental questions, and answering them would take us closer to providing a microscopic interpretation of the TMO effect. Being able to predict the TMO for different molecular structures would expand our ability to manipulate fluids with thermal gradients.

Previous work by different authors indicates that density gradients alone can lead to a preferred molecular orientation. A liquid-vapor interface is an example of a system featuring a sharp density gradient. It is well known that water molecules reorient at an interface, an effect that is often interpreted as a result of the maximization of the number of hydrogen bonds per molecule [16–18]. It has also been shown that polar and non-polar homonuclear dumbbells feature a tendency to orient with their bond axis parallel to the liquid-vapor interface [19, 20]. One question we would like to address is whether the density gradient induced by a thermal gradient may contribute to some degree to the molecular orientation. We have therefore endeavoured to extend our simulations to investigate molecular fluids confined by lyophobic walls, where the fluid has a weak tendency for adsorption. This simulation set-up allows us to introduce density gradients by imposing a "gravity"-like force on all of the fluid atoms, hence inducing a density gradient of varying magnitude. Furthermore, the examination of the density gradient and orientational effects induced by the applied force and thermal gradients acting both in concert and in opposition provide a route to disentangle the roles of density and thermal gradients in the TMO effect.

Our paper is structured as follows. In Section II we present an extension of the non-equilibrium thermodynamics (NET) theory previously developed to understand TMO. This implementation of the theory takes into account gravity-like forces and their corresponding coupling effects. In Section III we describe the force fields and the computational details of the molecular dynamics simulations performed in this work. In Section IV we present our results and discuss their interpretation, followed by our conclusions and final remarks

in Section V.

II. THEORETICAL BACKGROUND

We discuss in the following the theory required to describe the non-equilibrium response of a molecular fluid when it is subjected to a thermal gradient and/or an external gravity-like force. The force pushes the particles against a wall inducing a density gradient, which arises regardless of the presence of a thermal gradient. A thermal gradient will also induce a density gradient, which can either act in concert with or in opposition to that induced by the external force. Anticipating the discussion below, we will show that the gravity-like force can be used to cancel the density variation that appears as a consequence of the thermal expansion of the fluid.

Our theoretical approach uses classical non-equilibrium thermodynamics [15], which has been shown to describe well the thermal orientation of polar and non-polar fluids [5, 9, 11, 14] that were investigated using non-equilibrium molecular dynamics simulations. To take into account the orientational degrees of freedom in the theory, we use the approach introduced in Ref. 5. We describe the orientation of the molecules in terms of an orientation vector $\vec{n}(\vec{r},t)$, and we define a harmonic potential energy, $E = (C/2)\,|\vec{n}(\vec{r},t)|^2$, which depends on the force constant C that determines the "persistence" of the molecular director in maintaining a preferred orientation. This approach is reminiscent of Landau's theory of phase transitions [21], where quadratic and fourth-order contributions in the order parameter are considered. In our case, $\vec{n}(\vec{r},t)$ is the order parameter.

The external force $\vec{F}$ acts to change the position and the orientation of each molecule. A new system-dependent parameter D describes the response of the orientation vector to the force, and it will in general depend on the molecular mass distribution and geometry. The total energy density E then becomes

$$E\,(\vec{r},t) = \frac{C}{2}\,|\vec{n}(\vec{r},t)|^2 - c(\vec{r},t)\vec{r}\cdot\vec{F} - D\vec{n}(\vec{r},t)\cdot\vec{F} \tag{1}$$

where $c(\vec{r},t)$ is the particle density at position $\vec{r}$ and time t. We can now write the entropy production for a single component fluid subjected to a thermal driving force and a constant

external force, $\vec{F}$ acting on all atoms, with the internal degree of freedom, $\vec{n}(\vec{r},t)$,

$$\sigma(\vec{r},t) = \frac{1}{T(\vec{r},t)}\frac{\partial E(\vec{r},t)}{\partial \vec{n}(\vec{r},t)}\cdot\frac{\partial \vec{n}(\vec{r},t)}{\partial t} - \frac{1}{T^2(\vec{r},t)}\vec{J}'_q(\vec{r},t)\cdot\nabla T(\vec{r},t) \quad (2)$$

$$= -\frac{1}{T(\vec{r},t)}\left[C\vec{n}(\vec{r},t) - D\vec{F}\right]\cdot\frac{\partial \vec{n}(\vec{r},t)}{\partial t} - \frac{1}{T^2(\vec{r},t)}\vec{J}'_q(\vec{r},t)\cdot\nabla T(\vec{r},t), \quad (3)$$

where $\vec{J}'_q$ is the "reduced" heat flow [15]. $\partial\vec{n}/\partial t$ represents the orientational flux describing the response of the molecules to the gradient [5]. The associated linear flux-force relations are given by

$$\vec{J}'_q(\vec{r},t) = -\frac{1}{T^2(\vec{r},t)}L_{qq}\nabla T(\vec{r},t) - \frac{1}{T(\vec{r},t)}L_{qn}\left[C\vec{n}(\vec{r},t) - D\vec{F}\right] \quad (4)$$

$$\frac{\partial \vec{n}(\vec{r},t)}{\partial t} = -\frac{1}{T^2(\vec{r},t)}L_{nq}\nabla T(\vec{r},t) - \frac{1}{T(\vec{r},t)}L_{nn}\left[C\vec{n}(\vec{r},t) - D\vec{F}\right]. \quad (5)$$

At the stationary state the heat flux can be written as

$$\vec{J}'_q(\vec{r},t) = -\left(L_{qq} - \frac{L_{qn}L_{nq}}{L_{nn}}\right)\frac{\nabla T(\vec{r},t)}{T^2(\vec{r},t)}. \quad (6)$$

The $L_{\alpha\beta}$ terms in the equations given above are the Onsager phenomenological coefficients describing the main transport coefficients ($\alpha = \beta$) and the coupling between the different fluxes and gradients ($\alpha \neq \beta$). As already noted in Ref. 9, equation (6) shows that the coupling effects between orientation and thermal gradients results in a reduction of the thermal conductivity since in the absence of orientational coupling the thermal conductivity would be defined by L_{qq} only.

In the absence of external force, $\vec{F} = 0$, the linear laws reduce to the equations derived in Ref. 5. As noted there, the assumption that the system reaches a stationary state and taking a time average $\langle\vec{n}(\vec{r})\rangle$ of the orientation leads to a linear equation connecting the average orientation with the thermal gradient,

$$\langle\vec{n}(\vec{r})\rangle_{F=0} = -\frac{L_{nq}}{CL_{nn}}\frac{\nabla T}{T}. \quad (7)$$

In the absence of a thermal gradient, $\nabla T = 0$ but for $\vec{F} \neq 0$ we get

$$\langle\vec{n}(\vec{r})\rangle_{\nabla T=0} = \frac{D}{C}\vec{F}. \quad (8)$$

In the general situation with both thermal gradients and the external forces acting on the fluid we get

$$\langle \vec{n}(\vec{r}) \rangle = \langle \vec{n}(\vec{r}) \rangle_{F=0} + \langle \vec{n}(\vec{r}) \rangle_{\nabla T=0} \,. \tag{9}$$

We will examine in this paper the three different physical scenarios summarized by Equations (7-9).

III. COMPUTATIONAL DETAILS

We have investigated a molecular fluid consisting of mass- or size-asymmetric diatomic molecules, following the models employed by our group in previous works [5, 8, 22]. The diatomic dumbbells interact *via* pairwise Lennard-Jones (LJ) interactions with well depth $\epsilon_{\rm LJ}$ and average atomic diameter $\sigma_{\rm LJ}$ (not to be confused with the entropy production defined previously). We used dimensionless reduced units (denoted by * superscripts) throughout all the simulations. Real units can be recovered by substituting parameters suitable for real molecules, for example for carbon monoxide, $\epsilon_{\rm LJ} = 0.352$ kJ mol^{-1}, $\sigma_{\rm LJ} = 0.32717$ nm, and $m_{\rm LJ} = m_1 + m_2 = 28$ g mol^{-1}. The interatomic bond length matches carbon monoxide [23], $d = 0.128$ nm or $d^* = d/\sigma_{\rm LJ} = 0.391$ in reduced units. The molecular bond is held fixed using the SHAKE algorithm [24]. The time step was set to 0.0005 in reduced units.

The atoms in each molecule have a size ratio σ_2/σ_1, with a mean atomic size $\sigma^*_{\rm LJ} = (\sigma_1 + \sigma_2)/(2\sigma_{\rm LJ}) = 1.0$, and a mass ratio $m_2/m_1 = m^*_2/m^*_1$ with the reduced molecular mass $m^*_{\rm LJ} = m^*_1 + m^*_2 = 2.0$. The well depths for each atom were kept the same (*ie.* $\epsilon^*_1 = \epsilon^*_2 = \epsilon^*_{\rm LJ} = 1$). Lennard-Jones interactions were computed with the truncated and shifted LJ potential, using $r^*_{\rm cut} = 2.5$ as the distance cutoff for pair interactions. All the simulations were performed using the LAMMPS simulations software [25].

A schematic comparing the simulation set-up for our previous work on TMO in bulk systems with the new set-up for a fluid confined between walls is shown in Figure 1. A simulation box with L_z approximately three times larger than $L_x = L_y$ was used, with the temperature gradient applied in the z direction. Two walls were placed at $z = 0$ and $z = L_z$. The molecule-wall interactions were modelled with the integrated Lennard-Jones 9-3 potential [18, 26], $U_{\rm wall}(z)$, which mimics the interaction of the molecular fluid with a crystalline solid made up of individual Lennard-Jones particles,

$$U_{\rm wall}(z) = \epsilon_{\rm wall} \left[\frac{2}{15} \left(\frac{\sigma_{\rm wall}}{z} \right)^9 - \left(\frac{\sigma_{\rm wall}}{z} \right)^3 \right] \tag{10}$$

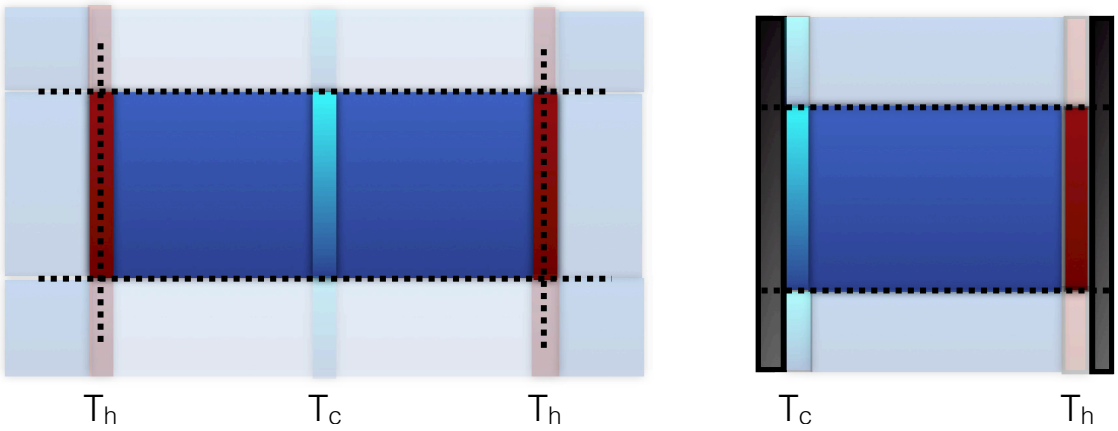

FIG. 1: Schematic representation of our implementation of a thermal gradient in 3D bulk fully periodic (left) and pseudo-2D confined (right) geometries. The latter is periodic in the x and y directions only. Red and blue colours show the regions where Langevin thermostats are applied to maintain hot and cold temperatures $T_{\rm h}$ and $T_{\rm c}$, respectively. The grey rectangles indicate the location of the confining walls

The interaction was computed between the wall and all individual atoms lying at a normal distance z from the wall. The wall potential is designed to mimic a lyophobic surface, with little fluid adsorption. We set the wall interaction parameters to $\epsilon_{\rm wall}/\epsilon_{\rm LJ} = 0.02$ and $\sigma_{\rm wall}/\sigma_{\rm LJ} = 0.6$. A distance cutoff of $2.5\sigma_{\rm LJ}$ was implemented in all of our computations.

The temperature gradients were generated by using Langevin thermostats in two regions near the walls located at $0 < z^* < 2.0$ and $L_z^* - 2.0 < z^* < L_z^*$. An average thermal gradient can be defined by the linear approximation $\nabla T_{\rm av}^* = (T_{\rm H}^* - T_{\rm C}^*)/(L_z^* - 4)$, with $T_{\rm H}^*$ and $T_{\rm C}^*$ being the temperatures of the hot and cold regions, respectively, but we note that the local thermal gradient may differ from the linear estimate, particularly if very large thermal gradients are applied. The average temperature of the non-equilibrium simulation is defined by $T_{\rm av}^* = (T_{\rm C}^* + T_{\rm H}^*)/2$. Upon application of the thermal gradient, the fluid develops a density gradient, which results from the thermal expansion of the fluid. For convenience to refer to specific simulation states we use an average density $\rho_{\rm av}^* = N_{\rm mol}/(L_x^* L_y^* L_z^*)$ and packing fraction $\eta_{\rm av}^* = \rho_{\rm av}^* \times V_{\rm mol}^*$, but our simulations do always involve a varying density, $\rho^*(z)$, unless it is stated explicitly otherwise.

A density and pressure gradient can also be created by simply adding a force in a direction perpendicular to the walls, which acts on each atom in the system. In our simulations the applied force had the form $F_{a,i}^* = m_i^* A^*$, with A^* being an effective acceleration. This

TABLE I: Summary of simulation parameters employed in this work

σ_2/σ_1	m_2/m_1	N_{mol}	$L^*_{x,y}$	L^*_z	ρ^*_{av}	η^*_{av}	T^*_{av}
2	1	770	10.45	32.0	0.22	0.274	2.28
1	20	770	8.0	25.0	0.48	0.391	2.43

force has the functional form of a gravitational force but must be many orders of magnitude times larger than the standard terrestrial gravity in order to compete with random thermal fluctuations in a simple molecular fluid. Typically we used values of A^* corresponding to about 10^{12} m/s^2 in real units. For comparison, the most powerful modern ultracentrifuges produce effective accelerations on the order of 10^7 m/s^2. For simulations at constant temperature, only, a Langevin thermostat was applied in the entire simulation box at the same time. We checked carefully that the temperature was homogeneous in the entire system. Representative temperature profiles supporting this point are reported in Section IV. We also verified that the principle of equipartition was upheld in all simulations by separately computing rotational and translational temperatures.

In Table I we summarize some of the simulation parameters employed in this work. All the simulations were performed at temperatures and densities far from the coexistence region of the models investigated. In selecting the thermodynamic conditions, which correspond to a dense supercritical fluid, we used information on the critical point obtained in our previous work [8]. Due to the weaker orientational response of the mass asymmetric model, for this model we chose to use parameters at lower temperatures and higher densities relative to the critical point, but always avoiding simulations inside the coexistence region. Using these parameters as a baseline, we then ran simulations in a range of different temperature gradients and/or with different applied forces. Simulation runs extended as long as required to obtain well converged results, generally on the order of 10^8 timesteps for each system.

IV. RESULTS AND DISCUSSION

A. Applied temperature gradient

We start our presentation with the simulation results for systems subjected to thermal gradients only. We show in Figure 2 the temperature and density profiles for systems

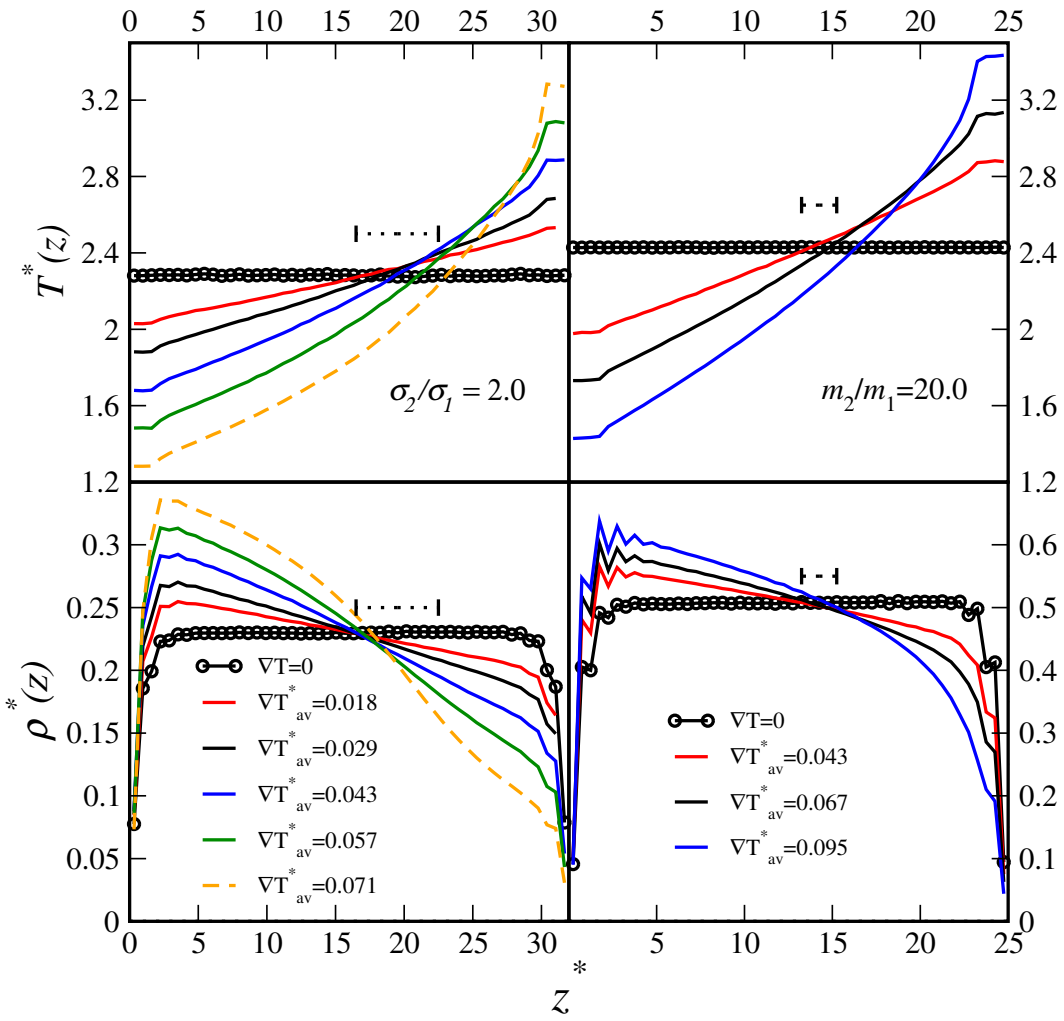

FIG. 2: Temperature (top) and density (bottom) profiles for size (left) and mass (right) asymmetric systems, for different temperature gradients, as a function of the z position across the simulation box. Horizontal dotted lines indicate the range in z^* over which average orientations were computed in the lower part of Figure 4.

featuring size or mass asymmetries. The temperature profiles show increasing deviations from linearity as the temperature gradient increases, in particular near the high temperature region. The density profiles clearly illustrate the lyophobic character of the wall associated with the weak fluid-wall interactions. This can be noted in the reduction of the density next to the wall. As expected the temperature and density (away from the interfacial region) profiles are flat for $\nabla T^*_{\rm av} = 0$.

The non-equilibrium simulations give direct access to the equations of state of the simulated systems. By plotting the pairs of density and temperature generated in the stationary

state it is possible to construct the equation of state. This approach has shown to provide excellent agreement with the equations of state obtained from equilibrium simulations in the isothermal isobaric ensemble [27]. It has also been shown that local thermal conductivities can be obtained, again showing excellent agreement with Green-Kubo equilibrium computations [28]. These results indicate that the non-equilibrium method employed here operates within the linear regime. See also below for a further discussion of this point.

We show in Figure 3 the equations of state obtained for the different states investigated in this work. The equations obtained are very similar to those we obtained previously in simulations of related systems of bulk fluids subjected to thermal gradients [8], except near the walls where depletion and/or molecular ordering induced by the walls play a significant role. The thermal expansion (slope of the curves represented in figure 3) also indicates that the states simulated here are either supercritical or in the liquid region. Some of the states at lower densities are closer to the critical point as can be seen from the sigmoidal shape of the equation of state. For the state closest to the critical point, in the size asymmetric system with $T_{\rm C}^* = 1.3$, the reduced critical temperature is 1.52 [8], but the density in the cold region, $\rho_{\rm C}^* \simeq 0.3$, is considerably above the reduced critical density of 0.15.

The anisotropy induced by the thermal gradient in the fluid, results in a preferred orientation of the molecules in the fluid with respect to the direction of the heat flux. In the top part of Figure 4 we show $\langle \cos \theta_z(z) \rangle$, the time-averaged variation in the average cosine of the angle θ_z between the molecular orientation vector $\vec{n}(\vec{r},t)$ and the heat flux vector (z axis), for the same systems shown in Figure 2. We arbitrarily set our molecular director to point in a direction such that the imposed thermal gradient generates a net negative orientation in both size and mass asymmetric systems, *i.e.* from the smaller/lighter atom to the larger/heavier atom.

Our results clearly show large deviations from isotropic orientations near the walls. This is particularly evident in the simulation performed in the absence of a thermal gradient, where any orientational preference is expected to be restricted to the fluid-wall interfacial region. Our simulations indicate that in the absence of thermal gradient the smaller atom in size asymmetric molecules tends to approach the wall more closely than the larger one. We note that as expected, in the absence of a thermal gradient there is no first order orientational preference for mass asymmetric molecules anywhere in the simulation box. In the presence of the thermal gradient for both systems the average orientation is anisotropic in the whole

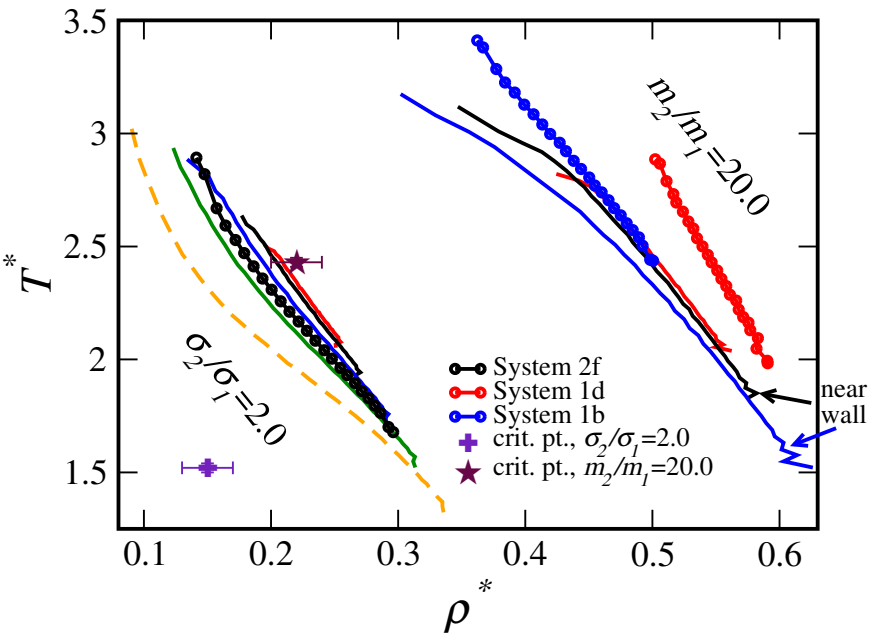

FIG. 3: Equations of state of fluids under thermal gradients. Labels (2f, 1d and 1b) correspond to data taken for the named systems in 3D bulk simulations in Ref. 8. The colours of the other lines lacking symbols are the same as the respective systems in Figure 2. Data points very near the walls have been omitted for clarity. We also indicate the critical points for the bulk systems taken from Ref. 8.

confined fluid, and in the size asymmetric case it is perturbed less overall in the center of the simulation box than near the walls. The direction of the anisotropy induced by the thermal gradient is consistent with our previous work, and the Soret coefficients computed in binary Lennard-Jones systems [5].

Following Equation 7, for a given thermodynamic state (defined by a specific temperature and density) we expect a linear dependence of the orientation with $\nabla T/T$. We show that this is indeed the case for the small thermal gradients investigated here (see Figure 4). The response to $\nabla T^*/T^*$ is expected to be linear, since $\nabla T^* T^{*-1} a^* \ll 1$ for thermal gradients in the range of $0.02 < \nabla T^* < 0.1$, $T^* \sim 2$ and the atom effective diameter $a \sim \sigma^* \equiv 1$, as is the case for all of the systems we consider in this study. However, if we increase the gradient beyond this upper limit it may become impossible to find a region in the systems where T^* and ρ^* are both nearly equal, as we would no longer be able to compare similar thermodynamic states. For this reason we have excluded the system with the largest thermal gradient ($\nabla T^*_{\rm av} = 0.071$) from the linear fit in the size asymmetric system.

From Equation 7 we can extract estimates of $L_{nq}(CL_{nn})^{-1}$ from the slopes of the plots in the bottom part of Figure 4. We get $L_{nq}(CL_{nn})^{-1} = 0.31$ for the size asymmetric case, and $= 0.13$ for the mass asymmetric case. The same thermal gradient induces a TMO effect 2.4 times larger in the size asymmetric system studied here compared with the mass asymmetric system. The strength of the TMO signal varies both with the thermodynamic conditions as well as the model parameters, as has been noted previously [8, 11, 12, 14, 22, 27].

B. Applied force

We have discussed above the thermal orientation behavior of confined molecular fluids under thermal gradients. Now we consider an alternative set up, where an external force is applied to induce a density gradient in the absence of a thermal gradient. Hence, we address in the following the situation described by Equation 8.

We show in Figure 5 the corresponding density and orientational profiles for the systems with an applied force, F^*. All these simulations were performed using Langevin thermostats to prevent the formation of temperature gradients, which may arise otherwise by the application of the external field. These density profiles are qualitatively similar to the profiles generated by the thermal gradient (cf. Figure 2). The main difference is some increase in the degree of molecular layering in the denser region near the wall at $L_z = 0$ observed in the simulations using the "gravitational" force. The molecular orientation is also qualitatively similar, with the larger site (in size asymmetric molecules) or heavier site (in mass asymmetric molecules) pointing in the direction of the density gradient.

The results presented above show that orientational anisotropy can be achieved by forcing a density gradient on the system in the absence of a thermal gradient. This observation is consistent with previous results on liquid-vapor interfaces of similar apolar dumbbells [19, 20], where large density gradients exist at equilibrium in the absence of thermal gradients, and lead to orientational effects driven by the surface tension. It follows from our results that the stronger the density gradient induced by the external force, F^*, the larger the molecular orientation. The degree of orientation, for the applied force and thermal gradient simulations, is found to be of the same order.

One question that stems from the analysis reported in this section is, how important is the density gradient in determining the overall degree of orientation of a system in a thermal

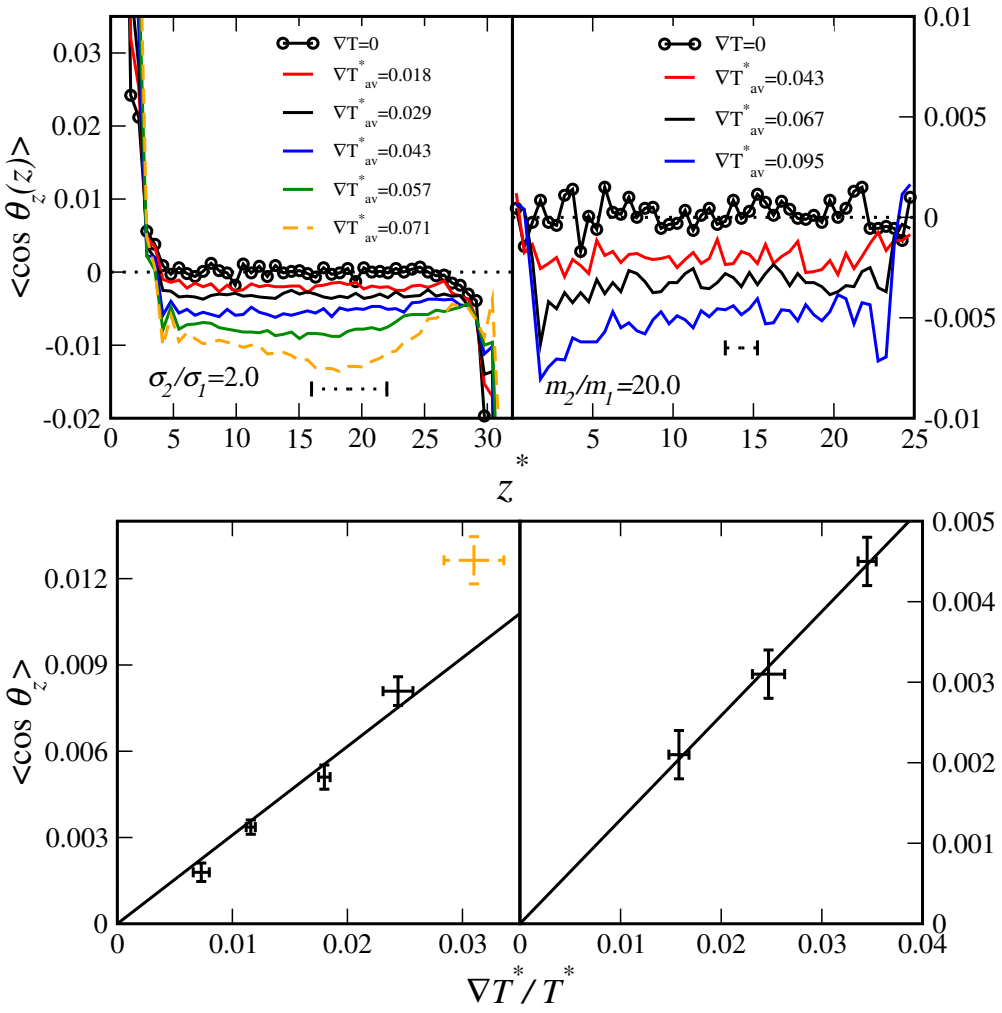

FIG. 4: (Top) Variation in the average molecular orientation of size and mass asymmetric fluids, as a function of the z position in the simulation box. (Bottom) Degree of orientation in the bulk region as a function of $\nabla T^*/T^*$. Points and error bars are derived from averages in a range of $16.5 < z^* < 22.5$ for size asymmetric systems and $13.25 < z^* < 15.25$ for mass asymmetric systems, shown as the horizontal dotted ranges in the top part of the figure. In the size asymmetric system (left) the data point for the largest thermal gradient (yellow dotted line/data point, both here and in Figs. 2 and 3) is not included in the linear fit.

gradient? We investigate this problem in the next section by performing simulations of systems under the influence of both external forces and thermal gradients.

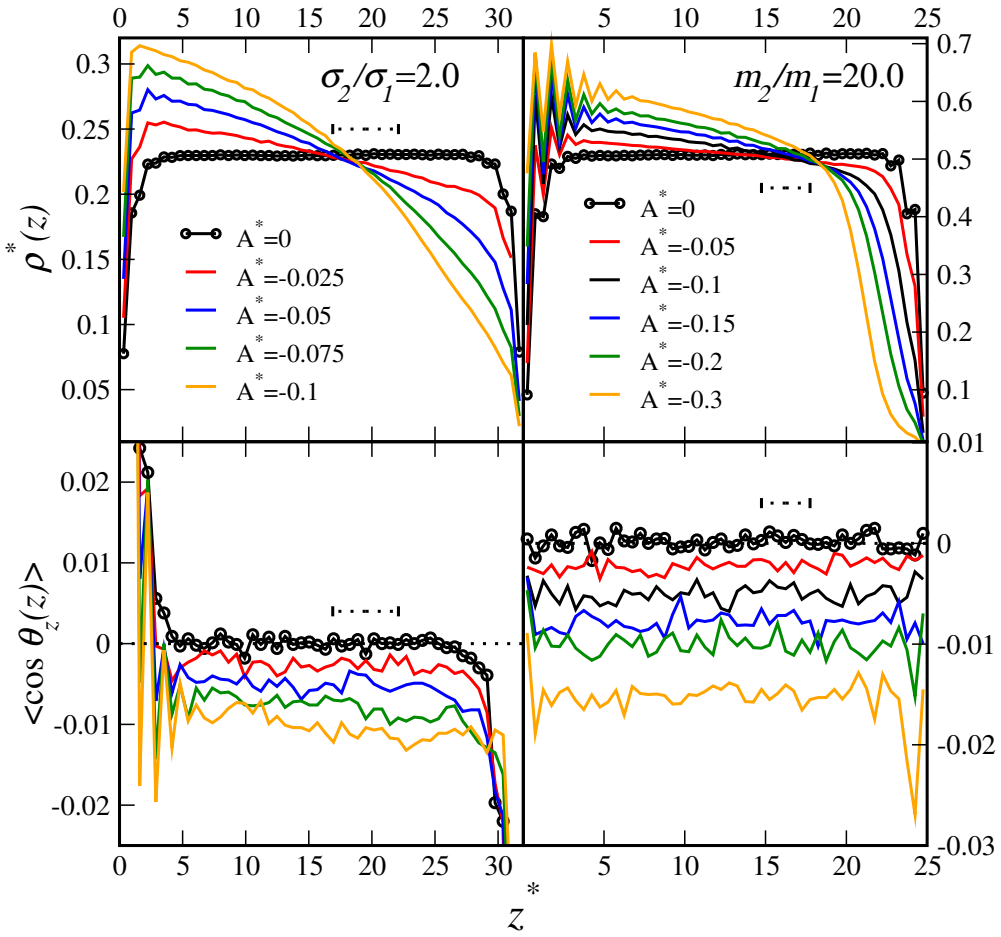

FIG. 5: Density profiles (top) and average molecular orientation (bottom) for confined fluids in different "gravitational" fields $F^*_{a,i} = m^*_i A^*$ and $\nabla T^* = 0$. The horizontal dotted line indicates the range in z^* over which the average orientations in Figure 7 were computed.

C. Application of temperature gradient and force in opposition

When the force is applied in the same direction as the thermal gradient, it will induce a density gradient in the opposite direction to that produced by the thermal gradient. We show some of the density profiles corresponding to this coupling in Figure 6. By carefully tuning the applied force, we can effectively cancel out the effect of thermal expansion on the density profile, leading to a situation where the density is constant in the bulk region away from the walls (see *e.g.* $A^* = 0.15$ system (green line) in Figure 6, top right).

In Figure 6 we also plot the resulting orientational profiles. As one would expect, in the middle of the simulation box the orientational responses driven by the two opposing influences of the applied force and the thermal gradient go in opposite directions, and we

find a reversal in the orientation between $A^* = 0.035 - 0.05$ and $A^* = 0.05 - 0.1$ for size and mass asymmetric systems, respectively. In Figure 7 we summarize our results for the average molecular orientation in a range of different applied temperature gradients and applied forces. The slopes of the lines in Figure 7 do not vary much regardless of the temperature gradient, demonstrating that for the range of parameters we study here, the two contributions to the orientation, F^* and ∇T^*, act independently.

According to Equations 8 and 9, a linear fit of the variation in the orientation as a function of applied force while keeping $\nabla T/T$ constant yields an estimate of the ratio D/C from the slope of the linear fit, which describes the strength of the coupling between the applied force and the molecular orientation. The average slope obtained from the set of lines in Figure 7 is 0.119 ± 0.006 in the size asymmetric case and 0.0514 ± 0.0010 in the mass asymmetric case. Since the molecular mass $m^* = m_1^* + m_2^* = 2$ in both systems, and the total force on each molecule $F_{\mathrm{mol}}^* = (m_1^* + m_2^*)A^*$, it follows that $D/C = 0.060 \pm 0.003$ for the size asymmetric system and 0.0257 ± 0.0005 for the mass asymmetric system. The coupling between the applied force and the molecular orientation is therefore about 2 times larger for the size asymmetric system investigated, nearly the same ratio as we obtained for the coupling to the thermal gradient (see Figure 4 and subsequent discussion above). While direct comparisons are difficult due to the differing average temperatures and packing fractions of the systems, it is clear that the relative contributions of the external forcing and the thermal expansion to the molecular orientation depend on the system parameters.

One important result that stems from our study is that in a system with zero density gradient there remains an overall effect on the orientational profile. In the bottom part of Figure 7 we show the average orientation in some of the same systems but as a function of the resultant density gradient. There is clearly a non-zero x-intercept, which we suggest is connected to an orientational bias that is due solely to the thermal gradient, since we have eliminated the influence of the density gradient. Furthermore the orientation in the mass asymmetric case is much larger than in the size asymmetric case with $\nabla \rho^* = 0$, showing that the exact balance between these two effects depends on the molecular geometry and thermodynamic conditions under consideration.

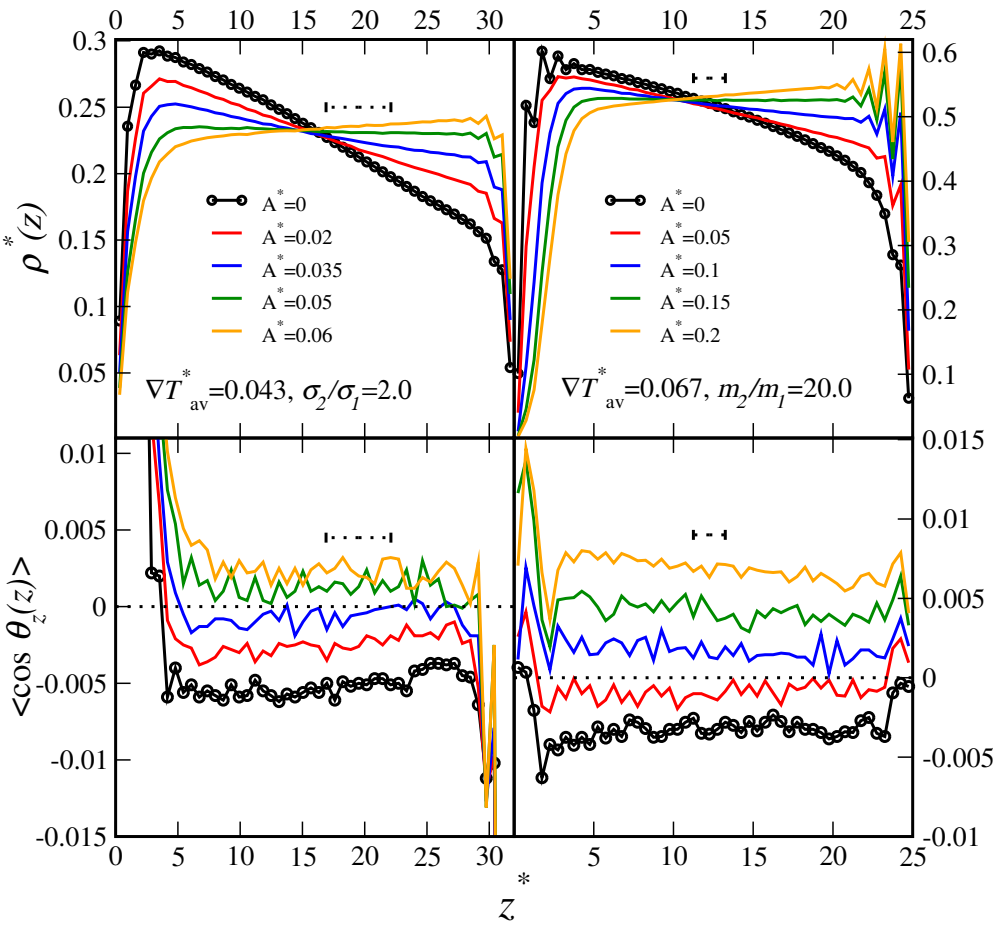

FIG. 6: Density profiles (top) and orientational profiles (bottom) under the simultaneous action of gravitational forces $F^* = m_i^* A^*$, and thermal gradients ∇T^*. The horizontal lines indicate the range in z^* over which the average orientations and density gradients in Figure 7 were determined.

V. CONCLUSIONS

We have investigated the non-equilibrium response of single-component diatomic fluids confined in lyophobic slit pores, under the influence of thermal gradients and/or gravity-like fields. The non-equilibrium thermodynamic (NET) analysis of this problem shows that mass gradients can also lead to molecular orientation, and the latter effect can contribute to the thermal orientation observed under a thermal gradient. We have shown that superimposed on this there are additional orientation effects due to the density gradient itself, provided that the fluid is asymmetric. Such effects could in principle be studied in a sufficiently powerful ultracentrifuge with a very large effective acceleration $g_{\rm eff}$, perhaps in a colloidal suspension of particles of large mass m and size σ so that the gravitational energy $mg_{\rm eff}\sigma$ can compete

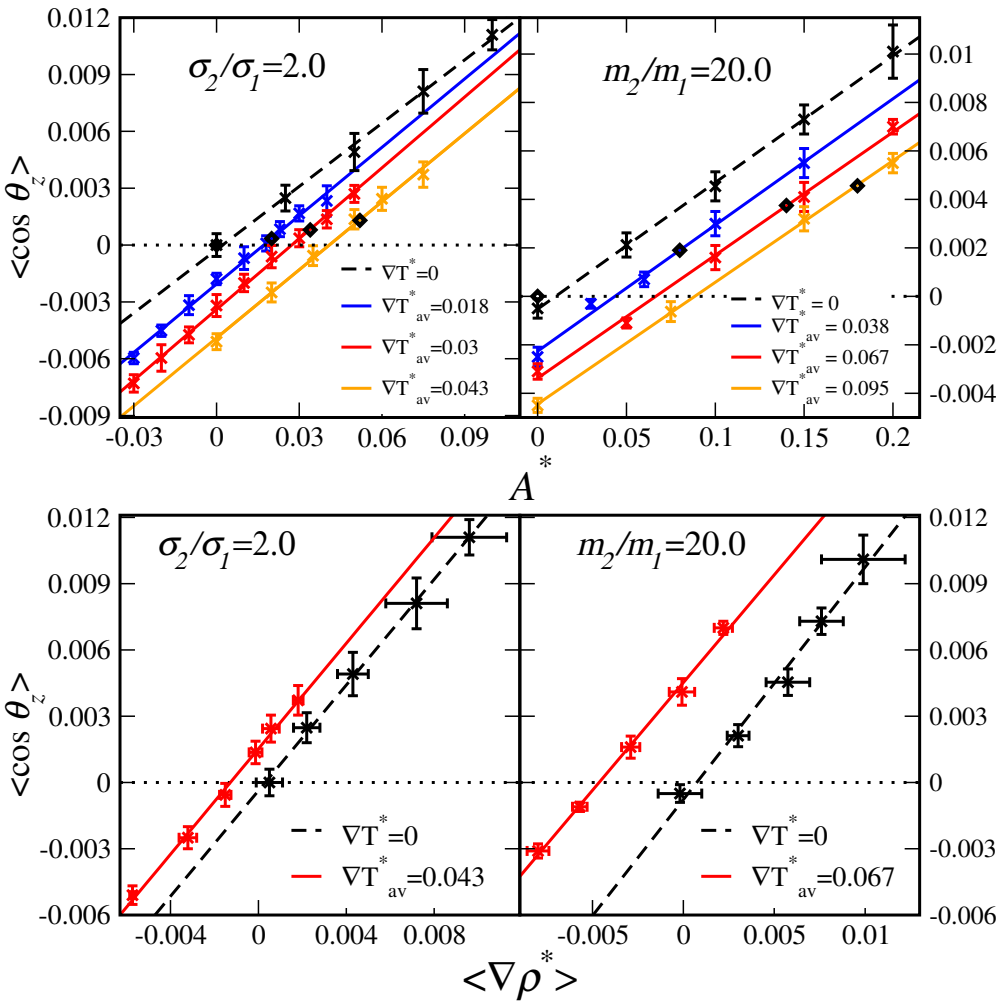

FIG. 7: Degree of orientation as a function of gravitational field strength A^* (top) and induced density gradient (bottom) at different average temperature gradients. Points and error bars are derived from averages over ranges in z indicated by the horizontal dotted lines in Figure 6. The diamonds in the top figure indicate the applied force required to produce zero density gradient in each temperature gradient.

with the thermal energy $k_{\mathrm{B}}T$. A fluid under a thermal gradient will inevitably develop a concomitant density gradient, whose origin is connected to the thermal expansion of the fluid. We have explored this idea by performing boundary driven non-equilibrium molecular dynamics (NEMD) simulations of molecular fluids consisting of diatomic molecules.

We find that, in both size and mass asymmetric dumbbells, the orientational bias caused by the application of a "gravitational" field, qualitatively resembles the orientation induced by thermal gradients. Furthermore, when the two driving forces ("gravitational" and ther-

mal) are applied together, they can act either in concert or in opposition and both determine the orientational preference of the fluid. Most importantly, we have shown that the opposed effects of the two external perturbations, on the molecular orientation on the one hand, and the density gradient on the other, do not exactly cancel out, so that *even under zero density gradient there remains an orientational bias that is purely driven by the thermal gradient.*

Overall, our work shows that thermal expansion plays a significant role in determining the magnitude of the thermal orientation of molecular fluids. Also, by combining the gravity-like force and thermal gradients, we have been able to disentangle thermal expansion and thermal gradient contributions, showing that the thermal orientation should be present in the absence of density gradients, or in fluids featuring small coefficients of thermal expansion. Our work advances our understanding of the microscopic mechanisms determining the non-equilibrium response and orientation of molecular fluids under thermal gradients.

Acknowledgments

We thank The Research Council of Norway (Project 221675) and the EPSRC (EP/J003859/1) for financial support, and NOTUR (account nn2920k) for computational resources. FB acknowledges the award of an EPSRC Leadership Fellowship and the Imperial College High Performance Computing Service for providing computational resources.

---

[1] F. Römer, Z. Wang, S. Wiegand, and F. Bresme, J. Phys. Chem. B **117**, 8209 (2013).

[2] C. D. Daub, D. Bratko, and A. Luzar, Top. Curr. Chem. **307**, 155 (2012).

[3] T. M. Squires and S. R. Quake, Rev. Mod. Phys. **77**, 977 (2005).

[4] E. Pop, Nano Res. **3**, 147 (2010).

[5] F. Römer, F. Bresme, J. Muscatello, D. Bedeaux, and J. M. Rubi, Phys. Rev. Lett. **108**, 105901 (2012).

[6] S. Wiegand, J. Phys. Condens. Matter **16**, R357 (2004).

[7] D. Reith and F. Müller-Plathe, J. Chem. Phys. **112**, 2436 (2000).

[8] C. D. Daub, P.-O. Åstrand, and F. Bresme, Phys. Chem. Chem. Phys. **16**, 22097 (2014).

[9] F. Bresme, A. Lervik, D. Bedeaux, and S. Kjelstrup, Phys. Rev. Lett. **101**, 020602 (2008).

[10] J. Muscatello, F. Römer, J. Sala, and F. Bresme, Phys. Chem. Chem. Phys. **13**, 19970 (2011).

[11] J. A. Armstrong and F. Bresme, J. Chem. Phys. **139**, 014504 (2013).

[12] J. A. Armstrong, A. Lervik, and F. Bresme, J. Phys. Chem. B **117**, 14817 (2013).

[13] J. Armstrong, C. D. Daub, and F. Bresme, J. Chem. Phys. **143**, 036101 (2015).

[14] J. Armstrong and F. Bresme, Phys. Rev. E **92**, 060103 (2015).

[15] S. R. de Groot and P. Mazur, *Non-Equilibrium Thermodynamics* (Dover Publications, Inc., New York, 1984).

[16] A. Luzar, S. Svetina, and B. Zeks, Chem. Phys. Lett. **96**, 485 (1983).

[17] A. Luzar, S. Svetina, and B. Zeks, J. Chem. Phys. **82**, 5146 (1985).

[18] C. Y. Lee, J. A. McCammon, and P. J. Rossky, J. Chem. Phys. **80**, 4448 (1984).

[19] S. M. Thompson and K. E. Gubbins, J. Chem. Phys. **74**, 6467 (1981).

[20] M. Mecke, J. Fischer, and J. Winkelmann, J. Chem. Phys. **114**, 5842 (2001).

[21] L. D. Landau and E. M. Lifshitz, *Statistical Physics* (Pergamon Press, Oxford, 1980).

[22] F. Römer and F. Bresme, Mol. Simul. **38**, 1198 (2013).

[23] M. Bohn, R. Lustig, and J. Fischer, Fluid Phase Equilib. **25**, 251 (1986).

[24] J. P. Ryckaert, G. Ciccotti, and H. J. C. Berendsen, J. Comp. Phys. **23**, 327 (1977).

[25] S. J. Plimpton, J. Comp. Phys. **117**, 1 (1995).

[26] F. F. Abraham and Y. Singh, J. Chem. Phys. **67**, 2384 (1977).

[27] F. Römer, A. Lervik, and F. Bresme, J. Chem. Phys. **137**, 074503 (2012).

[28] F. Bresme and J. Armstrong, J. Chem. Phys. **140**, 016102 (2014).

TOC graphic